Supporting Information

Enrichment and Detection of VEGF165 in Blood Samples on a Microfluidic Chip Integrated with Multifunctional Units

Xinyu He[abd], JunYan Xu[abd], Xiaoli Wang[acd], Chuang Ge[e], Shunbo Li[acd], Li Wang[acd], Yi Xu[*acd]

[a] Key Disciplines Lab of Novel Micro-Nano Devices and System Technology, Key Laboratory of Optoelectronic Technology and Systems, Ministry of Education, Chongqing University, Shapingba, Chongqing 400044, PR China

[b] School of Chemistry and Chemical Engineering, Chongqing University, Shapingba, Chongqing 400044, PR China

[c] School of Optoelectronic Engineering, Chongqing University, Shapingba, Chongqing 400044, PR China

[d] International R & D center of Micro-nano Systems and New Materials Technology, Chongqing University, Shapingba, Chongqing 400044, China

[e] Key Laboratory of Translational Research for Cancer Metastasis and Individualized Treatment, Chongqing University Cancer Hospital, Chongqing 400030, PR China

* Corresponding author at: Key Disciplines Lab of Novel Micro-Nano Devices and System Technology, Chongqing University, No. 174, St. Shazhengjie, Shapingba District, Chongqing, China.

E-mail addresses: xuyibbd@cqu.edu.cn (Y. Xu)

SI-1. Materials and methods

1. 1 Fabrication of the multifunctional microfluidic chip

The designed multifunctional microfluidic chip had a diameter of 10 cm, including the chip negative, adhesive film, chip channel layer, adhesive film, chip cover and cellulose nitrate film CN 140 stacked together from bottom to top (Figure S1). The thickness of three layers of PMMA was 1 mm, and the thickness of two layers of the adhesive film was 50 μm. The microchannel size of the chip middle layer was marked as shown in Fig S1B, and the size unit was mm.

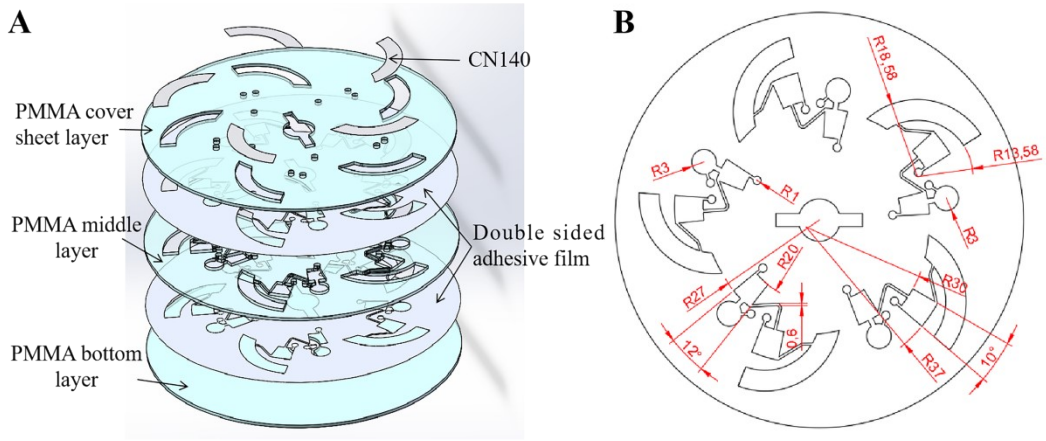

Figure S1. Schematic of the multifunctional microfluidic chip (A), Dimensions of microchannels of the chip (B)

1.2 The experimental setup and the supporting equipment

The center of the multifunctional microfluidic chip was engraved with fixing hole for matching the centrifugal rotor. The chip was placed on the centrifuge shown in Figure SI-2 (A) after adding blood, and the blood pretreatment process was completed driven by the centrifugal force. The detection equipment was shown in Figure SI-2 (B). The multifunctional microfluidic chip was placed on the stage of the fluorescence microscope to perform fluorescence detection on the enrichment and detection zone of the chip. The fluorescence spectrogram was displayed through the computer spectrometer operation software, and the subsequent data processing was performed.

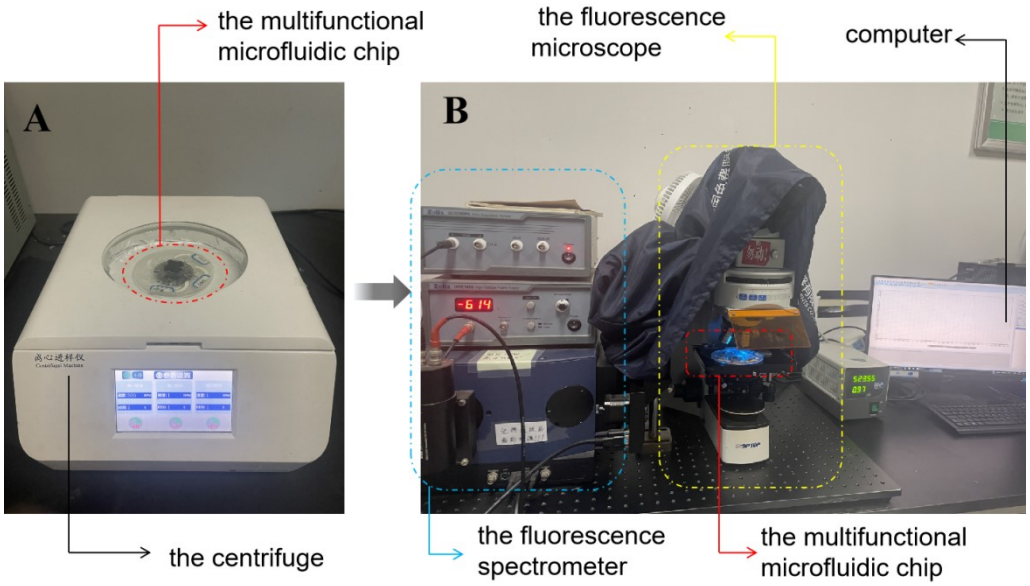

Figure S2. The centrifuge (A) and the fluorescence spectrometer with fluorescence microscope (B)

SI-2. Results and discussion

2. 1 Pretreatment of blood sample on the multifunctional microfluidic chip

2. 1.1 Plasma separation in the centrifuge separation zone

Due to the different densities of blood components, it is quite easy to separate blood cells and plasma by centrifugal rotation. When the centrifugal speed was too high (＞700 rpm), plasma and blood cells enter the ATPS mixing zone (Figure S3A) in advance, causing blood cells to pollute the ATPS solution and interfering with subsequent detection. When the centrifugation speed was 600 rpm, the separation status of plasma with different centrifugation time was shown in Figure S3B. At the 7th minute, plasma was no longer separated, which proved that the plasma and blood cells had been completely separated at the 6th minute. Therefore, in order to ensure the complete separation of plasma and blood cells and save time, the best centrifugal condition for plasma separation was 600 rpm and 6 min.

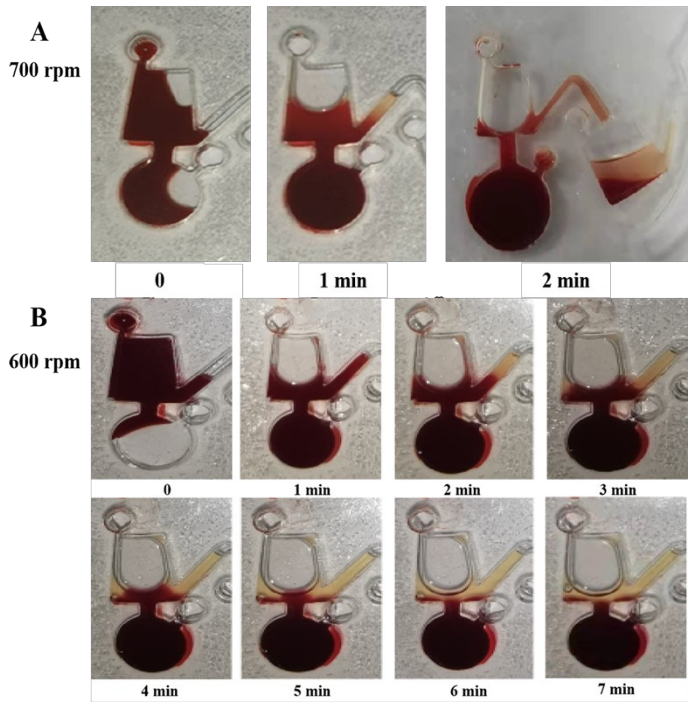

Figure S3. Plasma and blood cells separation obtained by blood centrifugation for different time under the condition of rotating speed of 700rpm (A) and 600rpm (B)

2.1.2 Effect of hydrophilicity of chip on plasma extraction

The microtube in the proposed multifunctional microfluidic chip used for plasma extraction was very narrow (600 μm wide). The effect of surface tension on the liquid could not be ignored. Therefore, the hydrophilicity of the chip surface was studied. The prepared PMMA surface was weakly hydrophilic (contact angle is 80.58° , Figure S4A). Before the bonding of each layer of the chip, the PMMA layers were cleaned with a plasma cleaner, and the hydrophilicity of the PMMA surface was enhanced (the contact angle was 22.03°, Figure S4B). The effect of plasma extraction with chips prepared by PMMA layers with different hydrophilicity was shown in Figure S4C and S4D. Under the same centrifugal conditions, the separated plasma could smoothly pass through the microchannel with enhanced hydrophilicity.

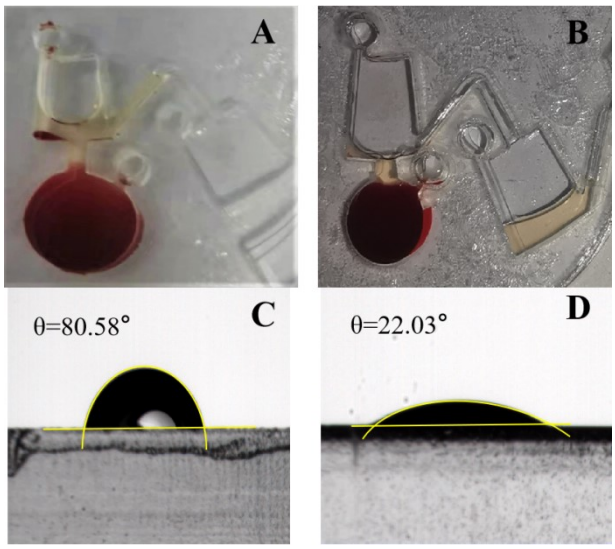

Figure S4. The chips prepared by untreated PMMA layer (A) and plasma cleaned PMMA layer (B)were used for plasma extraction and determination of their contact angles (C) and (D)

2.1.3 Extraction of the separated plasma

The chip prepared by PMMA layers with enhanced hydrophilicity was used to extract plasma, and the centrifugation conditions for plasma extraction were optimized. As shown in Figure S5A and S5B, plasma could not enter the ATPS mixing zone after centrifugation for at 500 rpm and 1000 rpm for 3 min. At 1500 rpm, plasma could enter the ATPS mixing zone after centrifugation for 3 min (Figure S5C). When the centrifugation speed was 2000 rpm and centrifuged for 2 min, the plasma could enter the ATPS mixing zone (Figure S5D). However, the ATPS solution in the mixing zone would enter the enrichment detection zone before it was completely mixed with plasma, affecting the detection effect. Therefore, in order to save time while fully mixing the separated plasma and ATPS solution, the best centrifugal condition for plasma extraction is 1500 rpm and 3 min.

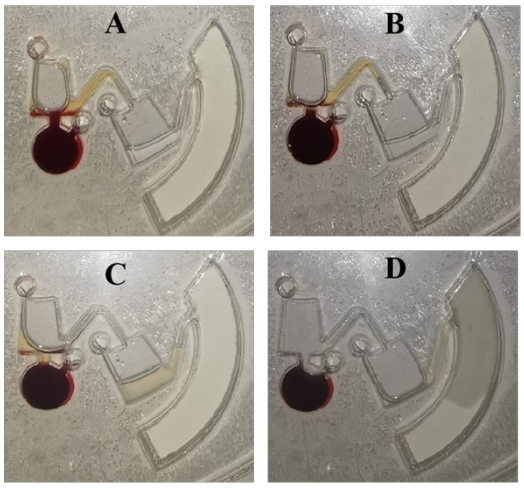

Figure S5. Plasma extraction of centrifugation at 500 rpm (A), 1000 rpm (B), 1500 rpm (C) and 2000 rpm (D) for 3 min

2.1.4 Transport of the ATPS mixture

After the separated plasma entered the ATPS mixing zone of the chip, the centrifugal force generated by the chip rotation would cause the plasma to mix with the aqueous two-phase system solution. At this time, $VEGF_{165}$ in plasma would be captured by AuNPs-Apt distributed in PEG phase. This process lasted for a short time. Subsequently, the mixture of separated plasma and ATPS was transported to the enrichment detection zone. The mixture was phase separated on CN140, and $VEGF_{165}$ was fully incubated with ZnO NPs-anti $VEGF_{165}$ and AuNPs-Apt. Here, the centrifugal conditions for the transport of ATPS mixture have been optimized. When the speed was 1500 rpm, 2000 rpm and 2500 rpm, the transfer time of ATPS mixture ass long (>6 min). As shown in Figure S6, at 3500 rpm, the ATPS mixture entered the enrichment detection zone after centrifugation for 3 min. Therefore, centrifugation for 3 min at 3500 rpm was the best transport condition for ATPS mixture.

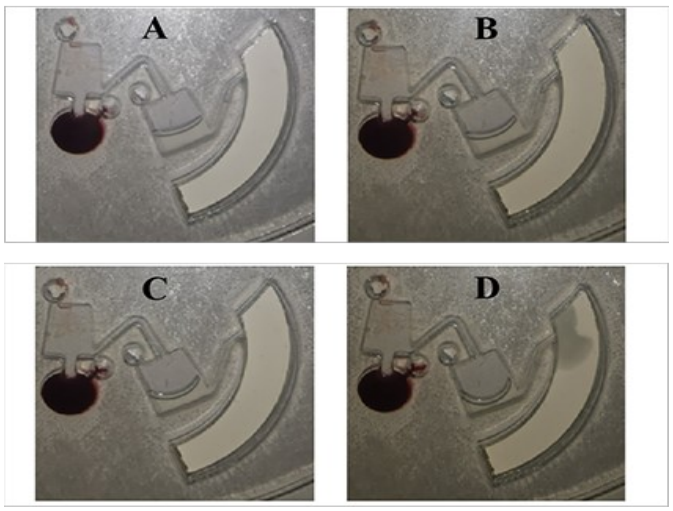

Figure S6. ATPS mixture transport of centrifugation at 3500 rpm for 0 (A)、1 min (B)、2 min (C)、3 min (D)

2. 2 Characterization of Au NPs and Au NPs-Apt

The synthesized Au NPs were characterized by TEM and DLS. The synthesized Au NPs were uniformly distributed with an average particle size of about 17 nm (Figure S7A). After the aptamer was coupled with Au NPs, the particle size increased to about 20 nm. There was a bright white area around the Au NPs, confirming that the surface of Au NPs has been covered by Aptamer (Figure S7B). The ultraviolet absorption of Au NPs is at 520 nm. When Apt was modified, the ultraviolet absorption peak of Au NPs-Apt had a red shift (Figure S7C), indicating that Apt had been successfully modified on Au NPs, and the addition of RhB would not affect the combination of Au NPs and Apt.

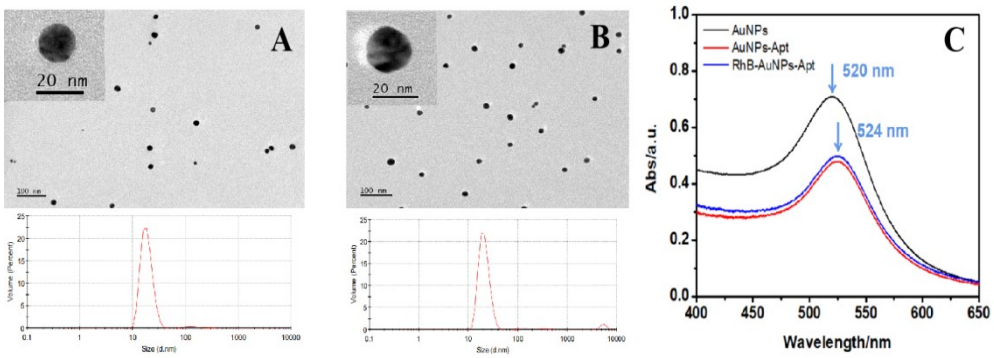

Figure S7. TEM and DLS characterization of Au NPs (A) and Au NPs-Apt (B), UV absorption spectra of Au NPs, Au NPs-Apt and RhB-Au NPs-Apt (C)

2. 3 Optimization of fluorescence detection conditions

In order to improve the fluorescence detection performance of the chip for $VEGF_{165}$, the concentration of anti $VEGF_{165}$ modified on the surface of CN 140/ZnO NPs was optimized. The results showed that with the increase of $VEGF_{165}$ concentration, the fluorescence difference (F_0-F) between negative and positive samples gradually increased. However, when the concentration of anti $VEGF_{165}$ exceeded 1 μg/mL, the fluorescence difference (F_0-F) decreased (Figure S8), which might be caused by the steric hindrance of excessive anti $VEGF_{165}$. Therefore, 1 μg/mL of anti $VEGF_{165}$ was selected as the best modification concentration.

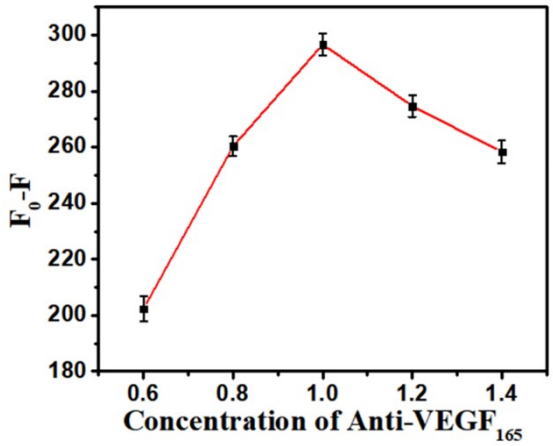

Figure S8. Optimization of the concentration of anti $VEGF_{165}$

After the ATPS mixture was transported to the enrichment detection area, the reaction time between the ATPS mixture and anti $VEGF_{165}$ on the surface of CN 140/ZnO NPs was investigated。As shown in Figure S9, when the reaction time was 60 min, the F_0-F between negative and positive samples was the largest, indicating that the capture rate of $VEGF_{165}$ was the largest at this time.

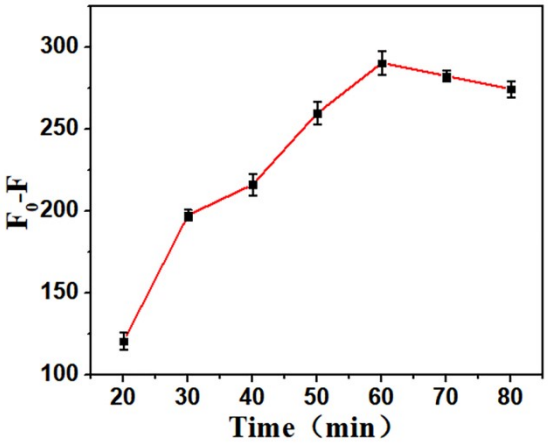

Figure S9. Optimization of incubation time of ATPS mixture on CN 140/ZnO NPs-anti $VEGF_{165}$

2. 4 Comparative testing of unknown samples

Table S1. Results of $VEGF_{165}$ detection in 3 unknown clinically blood samples

Unkown sample	ELISA kit (pg/mL)	The multifunctional microfluidic chip (pg/mL)	Analytical recovery (%)
1	409.34	394.10	96.3

2	53.21	50.02	94.0
3	127.66	119.58	93.7